Radar cross-section (RCS) analysis of high frequency surface wave radar targets

Gonca ÇAKIR[1]**, Levent SEVGİ**[2]
[1]*Electronics and Communication Engineering Department, Kocaeli University, Kocaeli-TURKEY*
[2]*Electronics and Communication Engineering Department, Doğuş University,*
Zeamet Sok. No 22, Kadıköy, İstanbul-TURKEY
e-mail: gonca@kocaeli.edu.tr, lsevgi@dogus.edu.tr

Abstract

Realistic high frequency surface wave radar (HFSWR) targets are investigated numerically in terms of electromagnetic wave – target interactions. Radar cross sections (RCS) of these targets are simulated via both the finite-difference time-domain (FDTD) method and the Method of Moments (MoM). The virtual RCS prediction tool that was introduced in previous work is used for these investigations. The virtual tool automatically creates the discrete FDTD model of the target under investigation and performs the FDTD RCS analysis. It also automatically constructs a MoM wire grid model of the target; therefore, it is also possible to compare FDTD results against the MoM-based NEC (Numerical Electromagnetic Code) data. Bi-static RCS patterns under a variety of illuminations over the whole HF band (3-30 MHz) are presented. The mono-static RCS vs. frequency of these targets is also given.

Key Words: *Electromagnetic scattering, High frequency surface wave radar, HFSWR, Surveillance, Radar cross-section, RCS, RCS prediction, RCS reduction, Finite-difference time-domain, FDTD, Method of Moments, MoM, Numerical electromagnetic code, NEC, mono-statics RCS, bi-static RCS, RCS pattern.*

1. Introduction

Radar systems designed to operate at high frequencies between 3 - 30 MHz are often classified as *over-the-horizon* (OTH) or *high frequency* (HF) radars because at such frequencies electromagnetic (EM) signals can reach beyond the line-of-sight (LOS) through the shadow region, traveling via either ionospherically refracted paths (called *sky waves*) or ground-coupled waves (called *surface waves*), where EM energy propagates along the Earth's curvature by diffraction. Such radar-to-target paths may extend from 50 to 3600 km in overall length, allowing surveillance of targets over large areas from relatively few radar sites. Targets include low-altitude missiles and aircraft, ships under way, and ballistic missiles during their boost phase [1-9].

Most military targets at HF have large radar cross sections (RCS), with an absolute free-space RCS ranging from a few m^2 (1-5 dB) to well over 1000 m^2 (30-50 dB). Specifically, at wavelengths of 10-60 m,

all manned aircraft fall into the Mie, or resonance, regime, and many such targets exhibit spans (wingspan or length) of one-half wavelength, resulting in RCS values that can approach λ^2, where λ is the wavelength. However at HF, the RCS of small aerial targets, such as unmanned air vehicles, can fall into the Rayleigh regime, where they act as a point reflector and their RCS values drop drastically [10,11].

The aim of this paper is to investigate RCS behaviors of *high frequency surface wave radar* (HFSWR) targets via numerical simulations. The simulations are performed via the recently introduced MGL-RCS virtual tool, which was summarized in a two-part paper [12-13]. The MGL-RCS is a three-dimensional (3D) finite-difference time-domain (FDTD)-based RCS analysis tool. The reader is referred to Part 1 of this paper [12] for the target reflectivity, RCS definitions, and tutorial material. The MGL-RCS numerical RCS prediction tool is presented in the second part [13]. The beauty of this tool comes from the fact that discrete FDTD and MoM models of realistic targets can be constructed automatically from 3D picture files (supplied in 3DS format). Also, custom-design 3D discrete targets (models) can be created from a few canonical blocks, such as the rectangular prism, cone, cylinder, sphere, and thoroid.

2. High frequency surface wave radars and surveillance

An option for the long range, wide area, ocean/sea surveillance of low-altitude air and surface targets is the HFSWR. HFSWR uses vertically polarized surface waves that follow the Earth's curvature, and, therefore, removes the LOS limitation of traditional microwave radars. Long ranges can be achieved because of the relatively low-attenuation of EM waves while propagating over the highly conductive ocean/sea surface. HFSWR can provide continuous, all-weather, 24-hour coverage in regions up to 200 nautical miles in range and $120°$ in azimuth. HFSWR is used not only in detecting and tracking targets, but also in supplying meteorological and oceanographic data [1-5].

Target detection in an HFSWR is handled in the Doppler domain. The total received echo contains information related to (1) surface and/or air targets, (2) EM wave – ocean/sea wave interaction (i.e., sea clutter), (3) noise, and (4) interference. HFSWR is a coherent device, and it discriminates between targets and any other undesired signals on the basis of their differing Doppler shifts (i.e., radial velocities). A target echo appears as primarily the result of scattering from vertical structures, and it will have a Doppler shift that is proportional to the target's radial velocity, which, in turn, is linearly dependent on the radar operation (carrier) frequency. The ocean/sea echo, although a continuum, is dominated by two large peaks, which are the result of Bragg resonant scatter [1-3]. Bragg lines have Doppler shifts that are proportional to the phase velocity of the Bragg-matched ocean waves; the phase velocity depends on the square root of the radar carrier frequency.

An HFSWR target signature is embedded in the signal environment, which is comprised of multiple sources of interference, dominated by high ocean/sea clutter and external noise limited. This signature (received signal) contains information due to the interaction between the EM waves and the target. EM wave - target interaction is classified in terms of the structure's dimensions and its relationship to the radar wavelength.

The RCS is a measure of the EM reflectivity of a target, which depends on the geometry, electrical properties, and the frequency. The three RCS frequency regimes where qualitative as well as quantitative differences occur are [10] (i) low frequencies (the *Rayleigh regime),* where the target's (*longest*) dimension (*l*) is much less than the radar wavelength ($l \quad << \quad \lambda$); (ii) medium frequencies (the *resonance regime),* where

the target dimension and the radar wavelength are of the same order ($l \approx \lambda$); (iii) high frequencies (the *optical regime),* where the target dimension is very large compared to the radar wavelength ($l >> \lambda$). The HFSWR wavelength is between 50 m and 100 m, therefore, the RCS region of interest is the *resonance regime.* In the resonance regime, the whole structure contributes to the target's RCS.

3.   The novel RCS virtual tool: MGL-RCS

The FDTD-based RCS prediction virtual tool, MGL-RCS, is designed in a way to automate almost the whole RCS analysis procedure. It has a useful Graphical User Interface (GUI) with features like 3D visualization, real time rotate, pan, and zoom. There are many tools to connect GUI elements to an application code. In this virtual tool, the Fox-toolkit, which is available under LPGL (Library GNU Public License), is preferred. FOX is a C++ based Toolkit for developing GUIs easily and effectively. It offers a wide and growing collection of Controls, and provides state of the art facilities such as drag and drop, selection, as well as OpenGL widgets for 3D graphical manipulation (visit www.fox-toolkit.org for more details).

The front panel of the MGL-RCS package is as given in Figure 1. At the top, besides the regular buttons, object design buttons are located. Any target can be designed with the help of rectangular, cylindrical, conical, spherical, and thoroidal blocks. The user can not only create original targets from these basic blocks, but can also insert custom-made images. The models are in 3DS format and may be downloaded from various internet sites. An ANSI-C library is used for image manipulation, lib3ds, working with the popular 3DS model format. Lib3ds is a free library, which simplifies the creation of 3DS import and export filters. All targets have PEC boundaries [13].
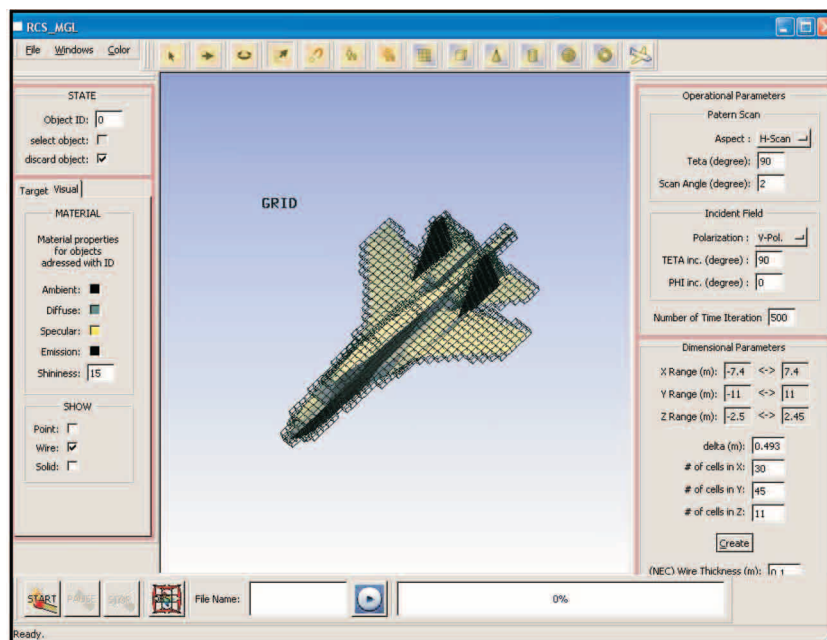

Figure 1. Front panel of the MGL-RCS package and 3D discrete model of an aerial target (SU-27 jet) imported from a 3DS file. It is discretized in a $30 \times 45 \times 11$ cell volume. The structural parameters are shown on the bottom-right block.

At the left, the parameters of the design window and target are given. The *State* block shows the status of the objects on the design window. *Base* represents the coordinate system; *OBS* is the near field observation plane. An object may be selected and discarded from this block. The *Target/Visual* block is beneath the *State* window. The user specifies the number of rows, columns and slices of any object, including the coordinate frame and the near field observation plane, together with actual width, depth, and height dimensions. An object or a group of objects can be relocated, re-scaled and rotated. Also, the picture on the design window can be zoomed in and out by using the right and left buttons of the mouse.

The two blocks on the right are used for operational parameters and model creation. In the *Operational Parameters* block, the incident field and RCS scan parameters are specified. Only vertical or horizontal scan is possible with this package. The scan angle is the angular resolution and supplied by the user. The number of time steps, i.e., the FDTD simulation period, is also supplied from this block (note that, for the structural parameters chosen in this package, 500 to 700 time steps are enough for the time domain simulations). In the *Dimensional Parameters* block, the sizes of the target are displayed. The user only supplies the cell size (Delta) in this block. Once it is given, the number of cells along each direction is displayed automatically.

The package creates both FDTD and NEC models of the target. The 3DS model and discrete FDTD and NEC2 models for a typical 52m-long, DC-10 aircraft are given in Figure 2. The model is meshed according to user-specified discretization parameters. Note that, the construction of these discrete FDTD and NEC models are the hardest part of numerical simulations using the FDTD and MoM techniques.
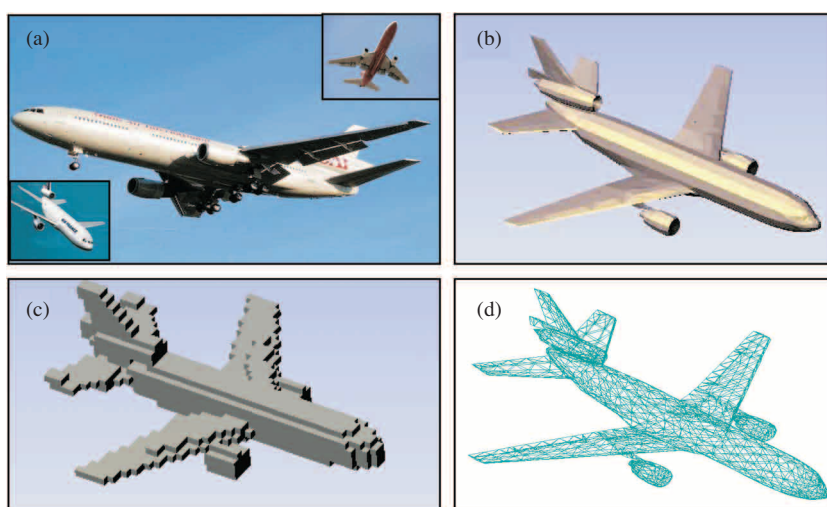

Figure 2. (a) A 52 m long DC-10 aircraft, (b) 3D DC-10 model pictured from a 3DS format file, (c) DC-10 discrete FDTD model, (d) DC-10 discrete NEC model extracted from the 3DS vertex information.

The FDTD model of the target is made up from a number of cubical cells. The output file RCS.PAR contains the FDTD model of the target together with the operational parameters. The NEC model contains the wire-grid model of the target. The wire grid model can be created either from the FDTD grid or from the 3DS vertex information [13]. In any case, after the creation of the discrete model of the target the user must save the file from the top menu (File Save). Note that, the number of FDTD cells and NEC segments should be increased in order to obtain more accurate discrete target models (with more details).

The buttons START, PAUSE and STOP are the run-time control buttons of the package. A very nice video-recording capability is added to the package. FDTD simulation is initiated once START button is pressed. The user then observes the incident field hitting the target from the specified direction, and the transient scattered fields all around the target on a specified observation plane. Pressing the RECORD button enables saving a video clip of the near scattered fields. Note that MGL-RCS can be used for multiple purposes: (i) any target may be designed or a target may be selected and loaded from a pre-listed 3DS files, (ii) time-domain near transient scattered fields can be simulated all around the target. To speed up the simulations in the second case, the near-to-far-field transformation (NTFF) module is not used [13]. A separate MGL-FDTD module is prepared for RCS prediction purposes.

The second module is the MGL-FDTD, which calculates near-fields in the time-domain using the FDTD method, and extrapolates far-scattered fields all around the target on a specified observation (either vertical or horizontal) plane with a given angular resolution. It also plots a number of angular RCS patterns at user-supplied frequencies by applying the discrete Fourier transformation (DFT) to the FDTD simulation data. The operational and target parameters are read from RCS.PAR and the output is recorded in a file named PLAIN.TXT. The output file contains multi-columns for the angle of scattering (θ_s and φ_s), theta- and phi-components of the scattered electric field, and the rectangular components of the near electric field (E_x, E_y, and E_z) at a point. The last module of the virtual tool MGL-PLOT may be used to produce 2D plots using the output file PLAIN.TXT. The user may plot time variations of the scattered fields along a specified direction, or RCS vs. frequency for both mono- and bi-static cases.

4. RCS Predictions with the FDTD and NEC simulations

Mono-static and bi-static RCS variations can be calculated via the FDTD and MoM simulations. Two types of plots may be generated: (1) backscatter RCS vs. frequency, and (2) bi-static horizontal RCS variations vs. angle. For the first case, the target is illuminated from a given direction, and the backscattered far fields are extrapolated. In the FDTD technique, this is simulated directly in the time domain, and a pulsed plane wave is used. Therefore, the broadband RCS signature is obtained via a single simulation. The plot of the backscattered RCS as a function of frequency is then obtained via off-line FFT analysis. In the MoM technique, the procedure must be repeated for a number of desired frequencies.

Bi-static RCS diagrams are obtained in a similar way in both the FDTD and MoM techniques. The target is illuminated from a given direction, and the scattered far fields are obtained in vertical or horizontal planes. Here, only horizontal diagrams are of interest. The scattered far fields are extrapolated at every $2°$, which means the extrapolation is carried out along 180 directions (from $\varphi=0°$ to $\varphi=360°$ with $\Delta\varphi=0°$ angular resolution). Each bi-static horizontal pattern also contains backscattered RCS information. After the FDTD simulation, the broadband co-polarized or cross-polarized RCS behavior is computed via off-line FFT analysis. Although any polarization can be chosen for the incident wave, in practice, vertically- or horizontally-polarized waves are used. Therefore, $\theta\theta$ and $\varphi\varphi$ co-polarization or $\varphi\theta$ and $\theta\varphi$ cross-polarization cases in RCS analysis can be explored with this package.

A commercial *NEC2* package [14] is used in MoM calculations. Here, any perfect electrically conducting (PEC) structure may be modeled in terms of short electrical dipoles. Wires are assumed to be a superposition of short segments. PEC planes are modeled in terms of wire meshes. Although metallic-facet models are available,

wire-grid models are more reliable in many open-source and commercial *NEC2* packages. Experience tells that the two have quite similar results when $\lambda/10$ or finer segmentation is used.

In all cases presented below, vertically polarized EM waves are used, and co-polarization in the horizontal plane (θ-polarization at $\theta=90°$) is taken into account. That is, the incident field has a vertical electric field component. Depending on the target, the scattered fields could have both horizontal and vertical electric field components. However, only the vertical electric field component was taken into account in the diagrams presented here.

Each bi-static pattern is normalized to its maximum, and maximum values of FDTD and NEC simulations are mentioned on the top left and right, respectively. The dynamic range of each plot is 30 dB, which means the distance between neighboring (dashed) circles is 6 dB. The angle of illumination is shown with an arrow. Parallel thick lines show the equi-phase surface of the incident plane wave. Incident and scattered field components that arc of interest are perpendicular to the paper. Therefore, these bi-static RCS patterns are the top view of the target's RCS behavior.

Note that FDTD yields near scattered fields in the time domain all around the target under investigation. Far fields are extrapolated via the NTFF routine. FDTD yields broadband transient EM effects if a Gaussian pulsed-plane wave is used as the incident wave. Once the user has this information, an off-line DFT may be applied to this time-domain data and a number of plots may be generated at different frequencies. On the other hand, NEC2 simulations must be repeated for each frequency, since MoM is a frequency-domain method. Finally, note that NEC2 package used in this paper gives the RCS as $\sigma_{dB}=10\text{Log}_{10}(\sigma/\lambda^2)$, therefore, one needs to add $10\text{Log}_{10}(\lambda^2)$ to the NEC2 results.
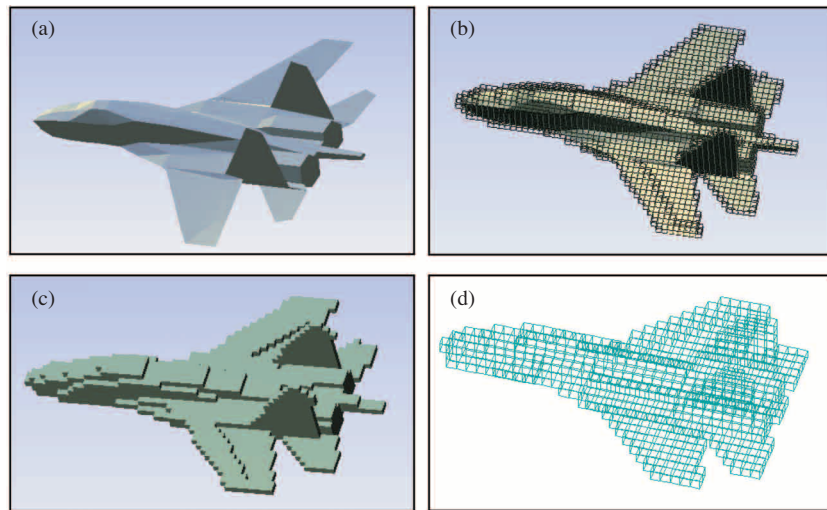

Figure 3. (a) The 3D model of a 22 m long SU-27 jet pictured from a 3DS file, (b) The 3DS model surrounded by a discrete shell used for FDTD discretisation, (c) The discrete FDTD model of the SU-27 jet, (d) The discrete NEC model of the SU-27 jet extracted from the discrete FDTD model. The number of cells in the FDTD model is 1259 and it occupies an FDTD volume of $30 \times 45 \times 11$ cells with the cell size of $\Delta x = \Delta y = \Delta z = 0.5$m. The NEC model uses 2804 wires.

5.   Characteristic examples with realistic HFSWR targets

Two real HFSWR targets are investigated in this section: a 22 m long SU-27 flanker air superiority fighter, and a 182 m long Virginia cruiser. The first RCS prediction example belongs to the SU-27 jet (see Figure 3). Figure 3a shows the 3DS graphics model of the jet. Figure 3b shows the status during the discretization process. The discrete FDTD and NEC2 models created in the MGL-RCS are shown in Figures 3c and 3d.

Video frames of these targets captured during the FDTD simulations are given in Figure 4. Here, near scattered EM fields at different time instants are shown. EM scattered waves all around the target are clearly observed in the figure. Figures 4a and 4b belong to a video recording of the SU-27 jet and Virginia cruiser. On top, the jet is shown. At the bottom, the cruiser is presented. Each frame is normalized to its maximum field value; therefore, different instant fields seem to have the same order. Observe the intensities of the tip and edge diffracted fields. Note that Figure 4b looks amazingly like inverse synthetic aperture radar (ISAR) images. They are very interesting, because they show the strength of the edge- and tip-diffracted waves, which are used to reconstruct the target from the scattered EM data.
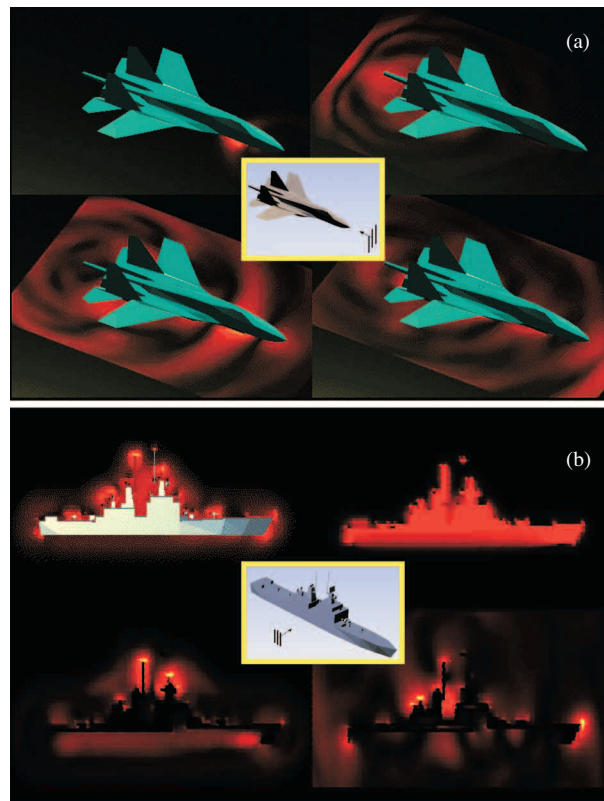

Figure 4. Near fields around two different targets captured during the FDTD simulations: (a) SU-27 jet, (b) Virginia (guided–missile) cruiser.

Figure 5 shows angular bi-static RCS patterns simulated with both FDTD and NEC packages at four different frequencies (3MHz, 5MHz, 15MHz and 30MHz). The agreement between FDTD and NEC2 results are quite impressive. It is interesting to note that the backscatter RCS of this 22 m long SU-27 jet is less than

0 dB at 3 MHz. This is because 22 m corresponds to $l \approx \lambda/4$ in the Rayleigh RCS regime. The jet acts like a point source with almost no significant backscattered field contribution. On the other hand, the backscatter RCS increases to 22-23 dB at 30 MHz. This is because the regime at this frequency is resonance.

Figure 6 shows the FDTD vs. NEC comparisons for the same target, but for a vertical scan. Note that the backscatter RCS is around 5 dB at 5 MHz, but increases to around 12 dB at 15 MHz.
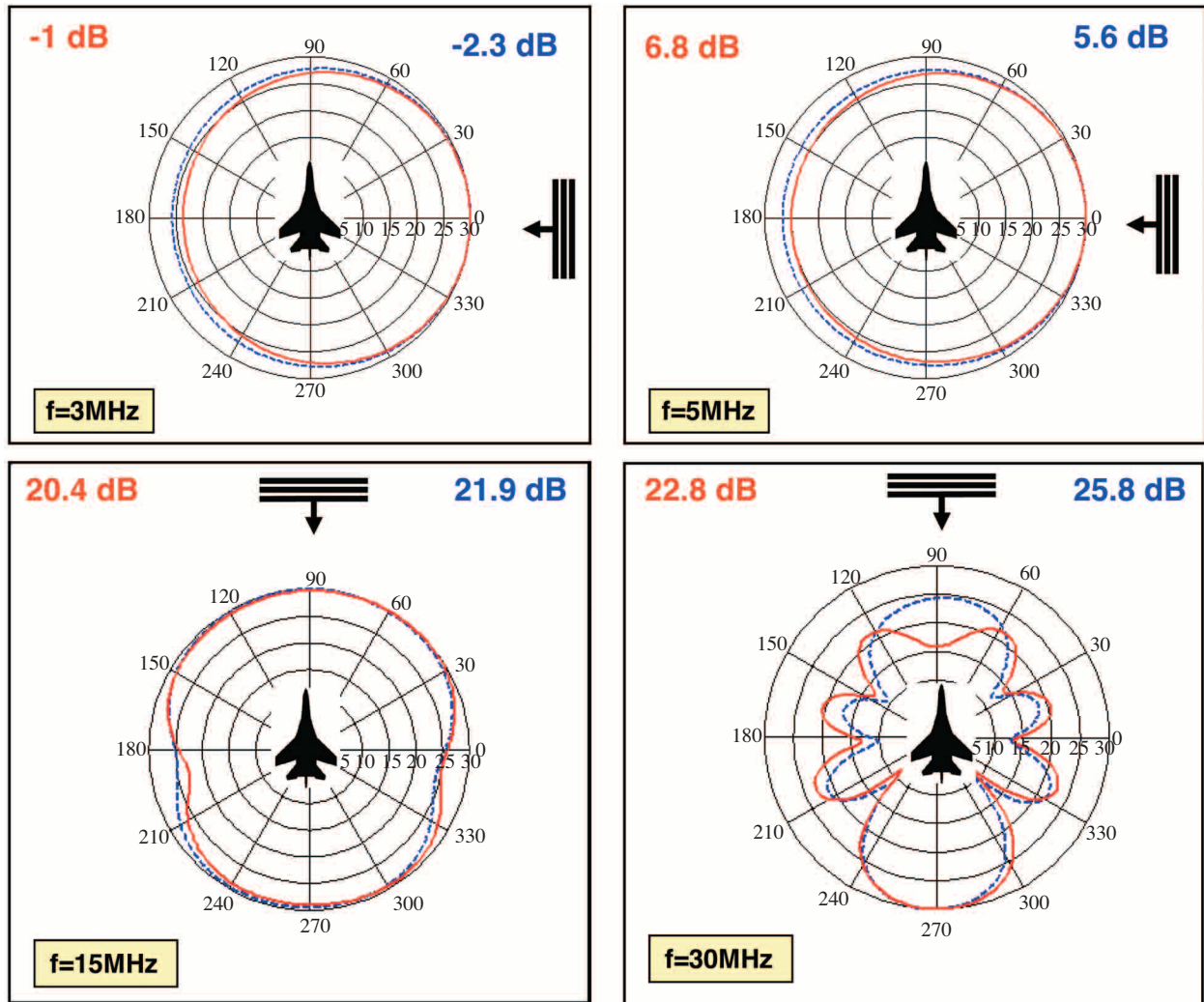

Figure 5. Angular bi-static RCS patterns simulated with both FDTD and NEC packages at four different frequencies ($\sigma_{\theta\theta}$ case). Real maximum values of FDTD and NEC2 simulations are given on top right and left, respectively. The angle of illumination is $\theta_i = 90°$, $\varphi_i = 0°$. The scattering angles are: $\theta_s = 90°$, $0° \leq \varphi_s \leq 360°$ with angular resolution of $\Delta\varphi = 2°$ (horizontal scan). Solid (red): FDTD, Dashed (blue): NEC2.

A mono-static (backscatter) co-polarized ($\sigma_{\theta\theta}$ case) RCS vs. frequency plot of the SU-27 is given in Figure 7. As can be observed, the backscatter RCS is less than 0 dB for frequencies less than 3 MHz. It resonates between 10 dB – 25 dB in the band of 5 – 25 MHz, and reaches 25 dB for frequencies higher than 25 MHz.
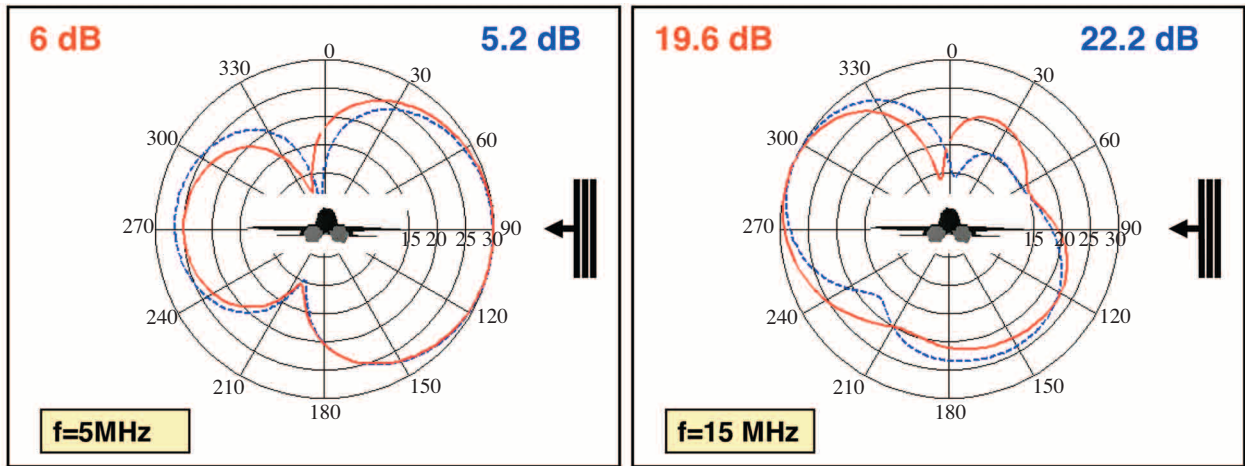
Figure 6. FDTD vs. NEC for angular bi-static RCS predictions fro vertical scan at two different frequencies ($\sigma_{\theta\theta}$-case): (a) f=5MHz, $\theta_i = 90°$, $\varphi_i = 0°$, $\varphi_s = 0°$, $0° \leq \theta_s \leq 360°$ Vertical scan, $\sigma_{\theta\theta}$-case. (b) f=15MHz, $\theta_i = 90°$, $\varphi_i = 90°$, $\varphi_s = 90°$, $0° \leq \theta_s \leq 360°$. Angular resolution is $\Delta\theta = 2°$. Solid (red): FDTD, Dashed (blue): NEC2.

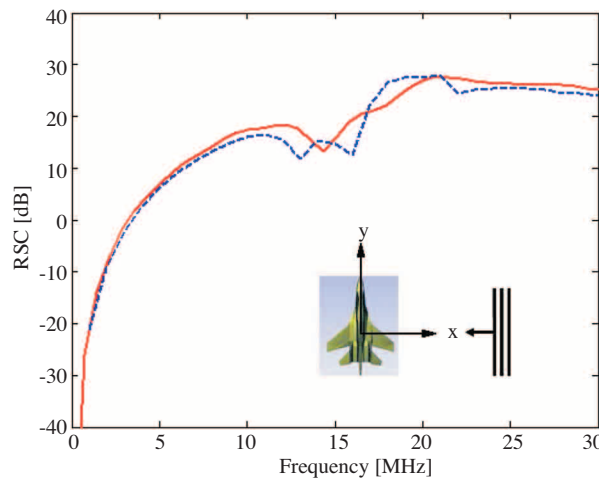**Figure 7.** Backscatter (mono-static) RCS vs. frequency variation of the SU-27 jet ($\theta_i = \theta_s = 90°$, $\varphi_i = \varphi_s = 0°$, $\sigma_{\theta\theta}$ case). The polarization is vertical. Solid: FDTD, Dotted: NEC2.

A 182 m long surface target, a Virginia guided - missile cruiser, is taken into account in the next example. Figure 8a shows both FDTD and NEC models of the 182 m long ship. The discrete FDTD model is made up 2298 cells and it occupies a target volume of $9 \times 80 \times 25$ cells. Since the package automatically adds 15-cells along each direction on both sides, the FDTD computation volume becomes $39 \times 110 \times 55$ cells. The dimensions of each cell are constant and are equal to $\Delta x = \Delta y = \Delta z = 2.27$m. The NEC model uses 6003 one-segment wires. Figure 8b and 8c show bi-static RCS patterns simulated with both FDTD and NEC packages at two different frequencies and illuminations. The RCS patterns are given at 5MHz and 15MHz. Both plots belong to the $\sigma_{\theta\theta}$ case (incident and scattered fields are Theta-polarized) and horizontal scan at $\theta_s = 90°$ with $\Delta\varphi = 2°$ angular resolution. Tests with different illumination at different frequencies show that bulk RCS of this 182 m long
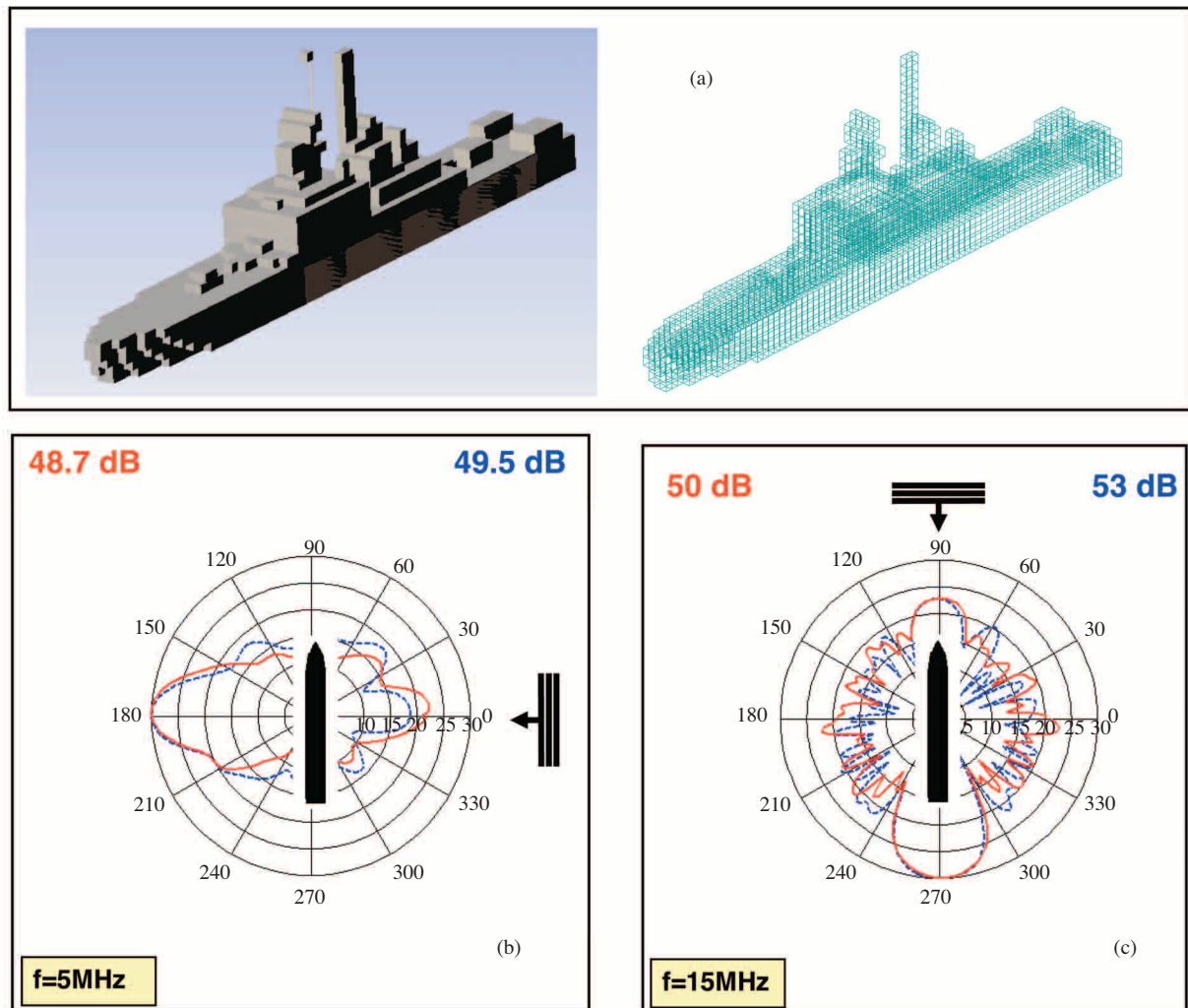
cruiser varies between 45 dB and 55 dB.

Figure 8. The 182 m long Virginia cruiser and FDTD vs. NEC comparisons for two different illuminations ($\sigma_{\theta\theta}$-case), horizontal scan ($\theta_s = 90°$, $0° \leq \varphi_s \leq 360°$): (a) The discrete FDTD and NEC models of the cruiser, (b) Angular bi-static RCS patterns at 5MHz ($\theta_i = 90°$, $\varphi_i = 0°$), (c) Angular bi-static RCS patterns at 15MHz ($\theta_i = 90°$, $\varphi_i = 90°$,. Angular resolution is $\Delta\varphi = 2°$. Solid (red): FDTD, Dashed (blue): NEC2.

6. Conclusions

Electromagnetic wave – targets are investigated numerically for the HFSWR systems. Two powerful RCS packages are used for this purpose. The first is an FDTD-based virtual RCS tool; the second is the well-known open source NEC code. Realistic air and surface targets with lengths varying from 10 m to 200 m are taken into account and RCS behavior is investigated from 3 MHz to 30 MHz over the whole HF band. It is observed that RCS values of as much as 55 – 60 dB may be obtained with these targets, depending on the illumination angle and polarizations.

References

[1] J.M. Headric and M. I. Skolnik. "Over-the-horizon radar in the HF band." in *Proceedings of IEEE*, Vol. 6, pp. 664-672, 1974.

[2] J. M. Headrick. "HF over-the-horizon radar." in *Radar Handbook*, 2nd ed., M. I. Skolnik, New York: McGraw-Hill, 1990.

[3] L. Sevgi. "Stochastic modeling of target detection and tracking in surface wave high frequency radars." *Int. J. of Numerical Modeling*, Vol. 11, No 3, pp.167-181, May 1998.

[4] L. Sevgi, A. M. Ponsford. "Multi-sensor, multi-resolution integrated maritime surveillance systems." inIEEE *Signal Processing and Applications Symp. (SIU'99)*, June 16-19, 1999, Ankara, Turkey.

[5] L. Sevgi, A. M. Ponsford. "Multi-sensor integrated maritime surveillance systems." in *IEEE International Multi-Conference on Circuits, Systems, Communications and Computers (CSCC'99)*, July 4-8, 1999, Athens, Greece.

[6] L. Sevgi, A. M. Ponsford, H.C. Chan. "An integrated maritime surveillance system based on surface wave HF radars, Part I – Theoretical background and numerical simulations." *IEEE Antennas and Propagation Magazine*, V.43, N.4, pp.28-43, Aug. 2001.

[7] A. M. Ponsford, L. Sevgi, H.C. Chan. "An integrated maritime surveillance system based on surface wave HF radars, Part II – Operational status and system performance." *IEEE Antennas and Propagation Magazine*, V.43., N.5, pp.52-63, Oct. 2001.

[8] L. Sevgi. "Stochastic modeling and simulation studies for the surface wave HF radar: Problems and challenges." in A Special Session on HF Radars, *Australian Int. Conference on Radar*, Sep. 3-5, 2003.

[9] L. Sevgi. *Complex Electromagnetic Problems and Numerical Simulation Approaches.* Piscataway, New Jersey: IEEE Press – John Wiley & Sons, 2003.

[10] L. Sevgi. "Target reflectivity and RCS interaction in integrated maritime surveillance systems based on surface wave HF radars." *IEEE Antennas and Propagation Magazine*, V.43, N.1, pp. 36-51, Feb. 2001.

[11] M. Çakır, G. Çakır, L. Sevgi. "Parallel FDTD-based radar cross section (RCS) simulations." in *Fifth International Conference on Electrical and Electronics Engineering (ELECO 2007)*, Dec 5-9, 2007, Bursa, Turkey.

[12] Ç. Uluışık, G. Çakır, M. Çakır, L. Sevgi. "Radar cross section (RCS) modeling and simulation: Part I – Definitions, strategies, and canonical examples." *IEEE Antennas and Propagation Magazine*, Vol. 50, No.1, pp.115-126, Feb 2008.

[13] G. Çakır, M. Çakır, L. Sevgi. "Radar cross section (RCS) modeling and simulation: Part II – A novel FDTD-based RCS prediction virtual tool." *IEEE Antennas and Propagation Magazine*, Vol. 50, No.2, pp.81-94, Apr 2008.

[14] G. J. Burke and A. J. Poggio. "Numerical electromagnetic code - Method of moments, Part I: Program description, theory." *Technical Document 116*, Naval Electronics System Command (ELEX 3041), July 1977.